PERGAMON

International Journal of Multiphase Flow 28 (2002) 1177–1204

International Journal of Multiphase Flow

www.elsevier.com/locate/ijmulflow

Modeling of phase inversion phenomenon in two-phase pipe flows

Neima Brauner *, Amos Ullmann

Department of Fluid Mechanics & Heat Transfer, Faculty of Engineering, Tel Aviv University, Tel Aviv 69978, Israel

Received 19 October 2000; received in revised form 13 January 2002

Abstract

Phase inversion in oil–water flow systems corresponds to the transitional boundary between oil-in-water dispersion and water-in-oil dispersion. In this study, the criterion of minimum of the system free energy is combined with a model for drop size in dense dispersions to predict the critical conditions for phase inversion. The model has been favorably compared with available data on the critical holdup for phase inversion. It also provides explanations of features of phase inversion phenomena in liquid–liquid pipe flows and in static mixers. © 2002 Published by Elsevier Science Ltd.

Keywords: Inversion; Liquid–liquid; Oil-water pipe; Two-phase

1. Introduction

Dispersed flow is a basic flow pattern frequently encountered in gas–liquid or liquid–liquid systems. Depending on the operational conditions, either of the two fluids involved can form the continuous phase. In oil–water two-phase flows there are water-in-oil (w/o) or oil-in-water (o/w) dispersions. Emulsion is a stable dispersion of fine droplets (w/o or o/w), which usually involves the presence of surfactants inhibiting coalescence of the dispersed droplets.

The phase inversion refers to a phenomenon where, with a small change in the operational conditions, the continuous and dispersed phase spontaneously invert. For instance, in oil–water systems, a dispersion (emulsion) of oil drops in water becomes a dispersion (emulsion) of water drops in oil, or vice versa. This transition is usually associated with an abrupt change in the rates of momentum, heat and mass transfer between the continuous and dispersed phases and between the dispersion and the system solid boundaries. Also, the drop size distribution of the dispersed

* Corresponding author. Tel.: +972-3-640-8930; fax: +972-3-640-8127.
E-mail address: brauner@eng.tau.ac.il (N. Brauner).

0301-9322/02/$ - see front matter © 2002 Published by Elsevier Science Ltd.
PII: S0301-9322(02)00017-4

phase depends on the type of dispersion. Therefore, a controlled phase inversion is a desirable and essential step in certain industrial processes. However, an uncontrolled phase inversion has to be prevented in all processes.

The phase-inversion is a major factor to be considered in the design of oil–water pipelines, since the rheological characteristics of the dispersion and the associated pressure drop change abruptly and significantly at or near the phase inversion point (Arirachakaran et al., 1989; Pan et al., 1995; Angeli and Hewitt, 1996). Also, the corrosion of the conduit is determined to a large extent by the identity of the phase that wets it.

The inversion point is usually defined as the critical volume fraction of the dispersed phase above which this phase will become the continuous phase. Studies have been carried out in batch mixers (e.g. Quinn and Sigloh, 1963; Clarke and Sawistowski, 1978; Selker and Sleicher, 1965; Norato et al., 1998; Groeneweg et al., 1998), continuous mixers (Tidhar et al., 1986), column contractors (Sarkar et al., 1980) and pipe flow (Arirachakaran et al., 1989; Nädler, 1995; Nädler and Mewes, 1997), in attempt to characterize the dependence of the critical volume fraction on the various system parameters, which include operational conditions, system geometry and materials of construction.

Most of the knowledge on phase inversion phenomenon comes from experiments carried out in stirred tanks. Selker and Sleicher (1965) defined an ambivalent range as the range of volume fractions of a phase above which that phase is always continuous and below which that phase is always dispersed. In the ambivalent range, either one of the two phases can be the dispersed phase. It is to be noted that the maximal dispersed phase holdup can exceed 74% (corresponding to maximal packing density of equal size spheres) and can go up to ≈90% (Pal et al., 1986; Guilinger et al., 1988). A primary factor which affects the limits of the ambivalent range seems to be the liquids viscosity ratio. Selker and Sleicher (1965) found that by increasing the oil phase viscosity, its tendency to be dispersed increases, whereby both the minimal oil volume fraction that can be continuous and its maximal volume fraction that can be dispersed increase. Also, the widest ambivalent range was obtained for liquids of about the same viscosities. The ambivalent range may also be influenced by other factors, such as the stirring speed, the wetting properties of the container material, liquids densities and surface tension. All these factors, as well as the initial conditions, were found to have a role in determining the location of the phase inversion point (within the ambivalent range) in a particular application (Mao and Marsden, 1977; Kato et al., 1991; Kumar et al., 1991; Kumar, 1996; Norato et al., 1998; Groeneweg et al., 1998; Yeo et al., 2000).

The tendency of a more viscous oil to form the dispersed phase is indicated by the data on dispersion inversion in pipe flows. It was found that the water cut required to invert a dispersion decreases as the oil viscosity increases. Based on the experimental results of various investigators on phase inversion, Arirachakaran et al. (1989) proposed the following correlation for the critical water cut, $\varepsilon_{\mathrm{w}}^{\mathrm{I}}$:

$$\varepsilon_{\mathrm{w}}^{\mathrm{I}} = \left(\frac{U_{\mathrm{ws}}}{U_{\mathrm{m}}}\right)_{\mathrm{I}} = 0.5 - 0.1108 \log_{10}(\eta_{\mathrm{o}}/\eta_{\mathrm{r}}); \quad \eta_{\mathrm{r}} = 1 \text{ mPa s} \tag{1}$$

where η_{o} is the oil viscosity, U_{ws} is the water superficial velocity and U_{m} is the mixture velocity. For highly viscous oils (above ≈0.2 Pa s) a constant value of $\varepsilon_{\mathrm{w}}^{\mathrm{I}} \simeq 0.15$ was reported (Brocks and Richmond, 1994).

Another empirical correlation was suggested by Nädler and Mewes (1997). Based on the momentum equations for stratified flow, assuming a negligible interfacial shear and no-slip between the two layers, the following equation was obtained:

$$\varepsilon_{\mathrm{w}}^{\mathrm{I}} = \frac{1}{1 + k_1 \left[\frac{C_{\mathrm{o}}}{C_{\mathrm{w}}} \frac{\rho_{\mathrm{o}}^{(1-n_{\mathrm{o}})}}{\rho_{\mathrm{w}}^{(1-n_{\mathrm{w}})}} \frac{\eta_{\mathrm{o}}^{n_{\mathrm{o}}}}{\eta_{\mathrm{w}}^{n_{\mathrm{w}}}} (DU_{\mathrm{m}})^{n_{\mathrm{w}}-n_{\mathrm{o}}} \right]^{1/k_2}} \tag{2}$$

where D is the pipe diameter, $\rho_{\mathrm{o,w}}$ and $\eta_{\mathrm{o,w}}$ are the densities and viscosities of the pure oil and water phases respectively, $C_{\mathrm{o,w}}$ and $n_{\mathrm{o,w}}$ are the parameters of the Blasius equation for the friction factor, CRe^{-n} and k_1, k_2, are empirical parameters. It was suggested that k_1 reflects the wall/liquids contact perimeter, as determined by the in situ configuration, and k_2 accounts for the flow regime in each of the phases. For laminar flow in both phases, and $k_1 = 1, k_2 = 2$, Eq. (2) is identical to the Yeh et al. (1964) model for the phase inversion point: $\varepsilon_{\mathrm{w}}^{\mathrm{I}} = 1/(1 + (\eta_{\mathrm{o}}/\eta_{\mathrm{w}})^{0.5})$. The later was developed with reference to a configuration of laminar flow in stratified layers, however, its validity was tested against the critical holdup data obtained in a flask (dispersion prepared by manual vigorous shaking of specified volumes of an organic and water phases).

In stirred tanks, the breakage of drops is due to the energy introduced into the system and turbulence created by the impeller. In column contractors and in pipe flows, the breakage forces are due to turbulent and viscous shear in the flow. In any case, for a stable liquid dispersion, a dynamic equilibrium between two competing phenomena of drops breakage and drops coalescence must be maintained. Depending in the physical properties of the fluids, the coalescence rate and the drop breakage rate (and the resulting drop size distribution) may be quite different in the initial dispersion and in the post-inversion dispersion. However, in both dispersions drop breakage and coalescence rates are in equilibrium.

Since phase inversion is a spontaneous phenomenon, it was proposed that its prediction can be based on the criterion of minimization of the total energy content of the system (e.g. Luhning and Sawistowski, 1971; Tidhar et al., 1986). The application of this criterion is, however, dependent on the availability of a reliable model for characterizing the drop sizes in the initial and post-inversion dispersions. Such models are challenged by the complexibilities involved in describing drops dynamic in dense dispersions, and in the case of mechanical mixers, also in a non-homogeneous flow field (Hoffer and Resnick, 1979; Gilchrist et al., 1989). Extensive investigations have been carried out over the years in order to explore the coalescence and break-up processes at both the micro-scale and macro-scale levels (e.g. Davies, 1992; Pacek et al., 1994; Brocks and Richmond, 1994; Gilchrist et al., 1989). These studies yield models for the collision frequency, coalescence efficiency and drop break-up (Shinnar, 1961; Chesters, 1991; Das et al., 1987), and attempts have been made to predict the critical conditions for phase inversion based on the drop dynamics as dominated by coalescence process (Arashmid and Jeffreys, 1980; Vaessen et al., 1996).

This study is motivated by the problem of phase inversion in pipe flows. In a recent paper (Brauner, 2001) a model for estimating the maximal drop size in dispersed flows has been derived by extending the Kolmogorov (1949)–Hinze (1955) model for the break-up of droplets in turbulent flow to the case of dense dispersions. This model has been successfully applied for predicting the critical operational conditions necessary for stabilizing dispersed flow patterns in gas–liquid and liquid–liquid systems. In this paper, this model is used together with the criterion

of minimization of the total system energy in order to predict the critical conditions for phase inversion in pipe flows and in static mixers.

2. Oil–water flow patterns maps

A typical flow pattern map for oil–water systems of $Eo_D = \Delta\rho g D^2/8\sigma \gg 1$ in horizontal tubes is shown in Fig. 1. Generally, these systems correspond to liquids with a finite density difference and sufficiently large tube diameter. For such systems, stratified flow with complete separation of the liquids (S) may prevail for some limited range of relatively low flow rates, where the stabilizing gravity force due to a finite density difference is dominant. With increasing the flow rates, the interface displays a wavy character with possible entrainment of drops at one side, or both sides of the interface (SM). The rate of droplet entrainment at the interface increases with increasing the liquids flow rates, and various flow patterns, which still involve stratification, may develop. These include a layer of oil-in-water dispersion above a water layer ($D_{o/w\&w}$) or a layer of water-in-oil dispersion with a free oil layer ($D_{w/o\&o}$). Layers of $D_{o/w}$ and $D_{w/o}$ may coexist ($D_{w/o\&o/w}$). The lighter and heavier phases may still be continuous at the top and bottom of the pipe, and are separated by a concentrated layer of drops at the interface, in that case, a three-layer structure is formed.

Inspection of experimental oil–water flow pattern maps reported in the literature reveals a general similarity between the sequence of flow patterns observed, but differences in the classification of the partially dispersed flow patterns (Brauner, 1998). The changes in the flow structure with increasing the water and/or oil flow rates may be gradual and the definition of these flow patterns and the associated boundaries are susceptible to subjective judgment and variations.

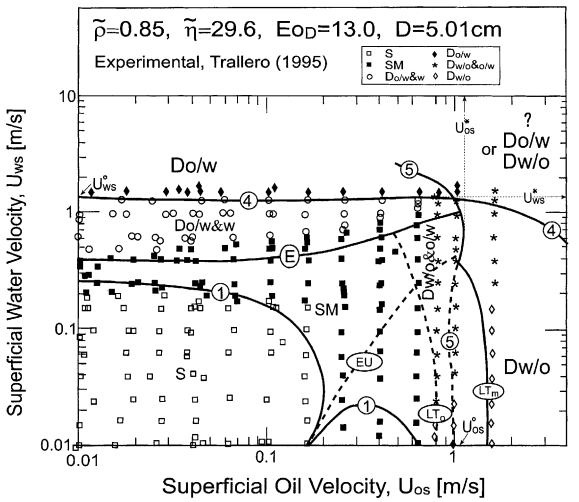

Fig. 1. A typical oil–water flow pattern map for horizontal system of $Eo_D \gg 1$: experimental data (Trallero, 1995) and models for predicting flow patters transition (Brauner, 1998, 2000, 2001). 1—neutral stability boundary for smooth stratified flow; E—entrainment of oil drops into the water layer; EU—equal velocity of fluids in stratified layers; LT_o—laminar/turbulent transition in the oil layer; 4—H-model, water continuous (Eqs. (5)–(12), $\tilde{C}_H = 1$); 5—H-model, oil continuous; LT_m—laminar/turbulent transition, oil continuous phase.

Nevertheless, models which consider the stability of the oil–water interface and the stratified flow structure (Brauner and Moalem Maron, 1992; Brauner, 1998) and the drops entrainment at the interface (Brauner, 2000) are capable of predicting the evolutions of the above partially dispersed flow patterns and the locus of transitional boundaries.

2.1. On the application of stratified flow models to phase inversion

Outside boundary 1 (Fig. 1), the linear stability theory predicts that a smooth interface of the stratified layers becomes unstable (Brauner, 1998). The evolution of interfacial waves gives rise to drop entrainment. When the water layer moves faster than the oil layer, oil drops are entrained into the water. Vice versa, with a faster oil layer, water drops are entrained into the oil layer. Consequently, flow patterns which involve a layer of $D_{o/w}$ are prominent in the zone where $U_w > U_o$ and those involving a layer of $D_{w/o}$ are expected in the zone where $U_o > U_w$ (and outside boundary 1). The conditions associated with $U_o = U_w$, as obtained via a stratified flow model, may thus imply transition from a region where entrainment is dominated by the water layer to a region where entrainment is denominated by the oil layer. It is worth noting that, with no-slip between the two layers ($U_o = U_w$), the in situ holdup corresponds to the input flow rates ratio.

Using the exact solution obtained for laminar flow between two infinite plates (e.g. Brauner et al., 1996a), the condition of $U_o = U_w$ corresponds to a critical ε_o^{EU} given by:

$$\varepsilon_o^{EU} = \frac{\tilde{\eta}^a}{1+\tilde{\eta}^a}; \quad \tilde{\eta} = \eta_o/\eta_w \tag{3}$$

with $a = 0.5$. This solution is in fact identical to the Yeh et al. (1964) model. Their solution for the critical holdup was derived based on the same stratified flow model with the condition of zero interfacial shear ($\tau_i = 0$). However, for this simple geometry of two infinite plates, the holdup obtained with $\tau_i = 0$ coincides with that obtained for $U_o = U_w$. This holdup is compared in Fig. 2a with the exact solution for ε_o^{EU} in laminar pipe flow with a plane interface (Brauner et al., 1996a). As shown in the figure, the conditions of $U_o = U_w$ in pipe flow correspond to higher ε_o ($a \simeq 1$ for $\tilde{\eta} \leqslant 10$ and it decreases for $\eta \gg 10$ to $a \simeq 0.8$). The solutions obtained using a two-fluid model (TF) for pipe flow (Brauner and Moalem Moron, 1989) are also shown in Fig. 2a. The results obtained depend on the model which is used to define the hydraulic diameters of the two layers. The FS model denotes the results obtained when the interface is considered as a free surface for both layers, whereas the SW model refers to the results obtained when the interface in the less viscous phase (water) is considered as a wall. As shown in the figure, the FS model is a significantly better approximation of the exact solution. All these laminar flow models assume a gravity dominated system, $Eo_D \gg 1$ (plane interface) and predict a critical holdup which is dependent only on the fluids viscosity ratio.

For turbulent flow in both layers, the effect of the viscosity ratio on ε_o^{EU} is moderated (Fig. 2b) and the fluids density ratio is an additional parameter. The results of the turbulent two-fluid model shown in Fig. 2b imply that:

$$\varepsilon_o^{EU} = \frac{\tilde{\eta}^a \tilde{\rho}^b}{1+\tilde{\eta}^a \tilde{\rho}^b}; \quad \tilde{\rho} = \rho_o/\rho_w \tag{4}$$

with $a \simeq 0.3$, $b \simeq 1.15$ (a, b obtained by linear regression of $\ln\left[(1/\varepsilon_o^{-1} - 1)\right]$ vs. $\ln(\tilde{\rho})$ and $\ln(\tilde{\eta})$).

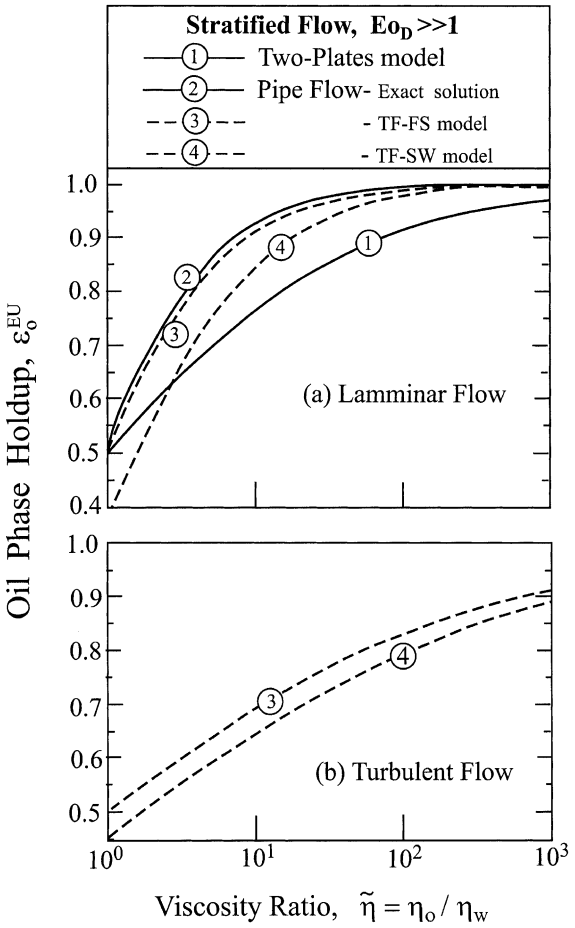

Fig. 2. Oil holdup (oil cut) corresponding to equal average velocities of oil and water in stratified flow, $Eo_D \gg 1$: (a) models of laminar stratified flow; (b) two-fluid turbulent model.

Apparently, for laminar flow, the solution for the ε_o^{EU} is independent on the fluids density ratio. However, the results shown in Fig. 2a and b correspond to a plane interface between the fluids, thus are valid for systems of $Eo_D \gg 1$. For $\tilde{\rho} \to 1$, $Eo_D \to 0$, surface forces become important and the liquids/wall wetting properties determine the interface shape (Brauner et al., 1996b; Gorelik and Brauner, 1999). For hydrophilic wall, the water/wall contact area increases and the interface tends to be concave (when water is the heavier phase). On the other hand, with hydrophobic wall, the interface is convex, whereby the oil layer contact area with the wall increases. Thus, in systems of low Eo_D, the solution obtained for ε_o^{EU} depends also on Eo_D (or the density ratio) and the liquids/surface wettability, which is represented by the contact angle, θ (Brauner et al., 1998).

Since, with hydrophilic wall, the water layer is slowed down, ε_o^{EU} becomes lower. On the other hand, with hydrophobic wall, the oil layer is slowed down and ε_o^{EU} increases. Eventually, in systems of $Eo_D \ll 1$ (capillary systems), the separated flow configuration is that of a fully eccentric core-annulus, with water in the annulus when $\theta \to 0$ (hydrophilic surface) and oil in the annulus

when $\theta \to 180°$ (Gorelik and Brauner, 1999). The exact solution, for ε_o^{EU} obtained for laminar flow in these configurations (Rovinsky et al., 1997) are shown in Fig. 3, in comparison to the exact solution obtained with a plane interface ($Eo_D \gg 1$). The results demonstrate the trends predicted for the variation of ε_o^{EU} with changing the tube material. However, these trends are opposite to the effect of the wall material on the critical holdup observed in real phase inversion. Experimental studies on phase inversion indicate a lower critical ε_o in hydrophobic container (pipe) surface, compared to that obtained in hydrophilic container (see, for example, Tidhar et al., 1986).

Although the equal-velocities (EU) line in Fig. 1 implies the location of transition from water-dominated to oil-dominated drop entrainment, it is not associated with a real phase inversion. The change in the drop entrainment process is rather gradual and the resulting flow patterns still exhibit stratification (layer of dispersion and a layer of oil or/and a layer of water). The opposite trend of the effect of the wall wetting properties on ε_o^{EU} is an indication that these models, which are based on stratified flow configuration, are not suitable for describing the critical conditions for phase inversion (although the model structure seems to be appropriate for correlating phase inversion data, as will be further shown in Section 3). Obviously, the phase inversion is the boundary between two fully dispersed flow patterns that are feasible in the flow system: oil-in-water dispersion and water-in-oil dispersion.

2.2. Dispersed flow boundaries

Fig. 1 shows that eventually, for sufficiently high water flow rates, the entire oil phase becomes discontinuous in a continuous water phase resulting in an oil-in-water dispersion or emulsion ($D_{o/w}$). Vice versa, for sufficiently high oil flow rates, the water phase can be completely dispersed in oil phase, resulting in a water-in-oil dispersion or emulsion ($D_{w/o}$). It is, therefore, the locus

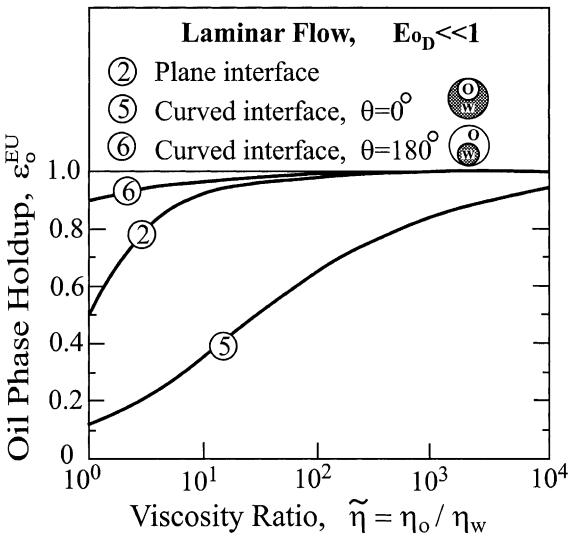

Fig. 3. The effect of the liquids/surface wetting on the oil cut corresponding to equal average velocities of oil and water layers in $Eo_D \ll 1$ systems.

of the phase inversion curve which ultimately defines the regions of stable $D_{w/o}$ and $D_{o/w}$. The maximal holdup of either stable ($D_{w/o}$ and $D_{o/w}$) is controlled by the phase inversion phenomena.

The model used to predict the dispersed flow boundaries (4 and 5 in Fig. 1) is the H-model presented in Brauner (2001). According to this model, a homogeneous dispersion can be maintained when the turbulence level in the continuous phase is sufficiently high to disperse the other phase into small and stable spherical droplets, with a maximal size, d_{max} smaller than a critical drop size, d_{crit}. The H-model consists of an extension of the Kolmogorov (1949)–Hinze (1955) model for d_{max} in a turbulent flow field, to account also for the effect of the dispersed phase holdup, ϵ_d. The relevant model equations are herein briefly reviewed.

The Hinze model is applicable for dilute dispersions. It suggests that the maximal drop size, $(d_{max})_0$, can be evaluated based on a static force balance between the eddy dynamic pressure and the counteracted surface tension force (considering a single drop in a turbulent field). In dense dispersions, where local coalescence is prominent, the maximal drop size, $(d_{max})_\epsilon$, is evaluated based on a local energy balance (Brauner, 2001). In the dynamic (local quasi-steady) breakage/coalescence processes, the turbulent kinetic energy flux in the continuous phase should exceed the rate of surface energy generation that is required for the renewal of droplets in the coalescing system. In dilute systems, this energy balance is trivially satisfied for any finite drop size (as the rate of surface energy generation vanishes for $\epsilon_d \to 0$) thus, $(d_{max})_\epsilon < (d_{max})_0$. However, this is not the case in the dense system where $(d_{max})_\epsilon > (d_{max})_0$.

Thus, given a two-fluid system and operational conditions, the maximal drop size is taken as the largest of the two values:

$$\tilde{d}_{max} = \max\left\{\left(\tilde{d}_{max}\right)_0, \left(\tilde{d}_{max}\right)_\epsilon\right\} \tag{5}$$

where $\left(\tilde{d}_{max}\right)_0$ is the (dimensionless) maximal drop size in a dilute dispersion:

$$\left(\tilde{d}_{max}\right)_0 = \left(\frac{d_{max}}{D}\right)_0 = 0.55\left(\frac{\rho_c U_c^2 D}{\sigma}\right)^{-0.6}\left[\frac{\rho_m}{\rho_c(1-\varepsilon_d)}f\right]^{-0.4} \tag{6.1}$$

and $\left(\tilde{d}_{max}\right)_\epsilon$ is the (dimensionless) maximal drop size in a dense dispersion:

$$\left(\tilde{d}_{max}\right)_\epsilon = \left(\frac{d_{max}}{D}\right)_\epsilon = 2.22\tilde{C}_H\left(\frac{\rho_c U_c^2 D}{\sigma}\right)^{-0.6}\left[\frac{\rho_m}{\rho_c(1-\varepsilon_d)}f\right]^{-0.4}\left(\frac{\varepsilon_d}{1-\varepsilon_d}\right)^{0.6} \tag{6.2}$$

where $\tilde{C}_H$ is a tunable constant, $\tilde{C}_H = O(1)$ and f is the wall friction factor. For instance, Blasius equation ($f = 0.046/Re_c^{0.2}$) yields:

$$\left(\tilde{d}_{max}\right)_0 = 1.88\left[\frac{\rho_c(1-\varepsilon_d)}{\rho_m}\right]^{0.4} We_c^{-0.6}\, Re_c^{0.08} \tag{7.1}$$

$$\left(\tilde{d}_{max}\right)_\epsilon = 7.61\tilde{C}_H We_c^{-0.6} Re_c^{0.08}\left(\frac{\varepsilon_d}{1-\varepsilon_d}\right)^{0.6}\left[1+\frac{\rho_d}{\rho_c}\frac{\varepsilon_d}{1-\varepsilon_d}\right]^{-0.4} \tag{7.2}$$

where $Re_c = \rho_c D U_c/\eta_c$ and $We_c = \rho_c U_c^2 D/\sigma$ (subscript c denotes the continuous phase). The H-model is applicable provided:

$$1.82Re_c^{-0.7} < \tilde{d}_{max} < 0.1 \quad \text{and} \quad Re_c > 2100 \tag{8}$$

For a homogeneous dispersion, applying the no-slip model yields the in situ holdup and the mixture density, ρ_m in terms the superficial velocities of the dispersed and continuous phases ($U_{ds} = Q_d/A$, $U_{cs} = Q_c/A$):

$$\varepsilon_d = \frac{U_{ds}}{U_{ds} + U_{cs}}; \quad U_c = U_d = U_{ds} + U_{cs} \equiv U_m \tag{9.1}$$

$$\rho_m = \varepsilon_d \rho_d + (1 - \varepsilon_d)\rho_c \tag{9.2}$$

The critical drop size, d_{crit} is taken as:

$$\frac{d_{crit}}{D} = \min\left(\frac{d_{c\sigma}}{D}, \frac{d_{cb}}{D}\right) \tag{10}$$

where $d_{c\sigma}$ represents the maximal size of drop diameter above which drops are deformed and thereby enhancing coalescence (Brodkey, 1969):

$$\tilde{d}_{c\sigma} = \frac{d_{c\sigma}}{D} = \left[\frac{0.4\sigma}{|\rho_c - \rho_d| g \cos\beta' D^2}\right]^{1/2} = \frac{0.224}{(\cos\beta')^{1/2} Eo_D^{1/2}} \tag{11.1}$$

$$Eo_D = \frac{\Delta\rho g D^2}{8\sigma}; \qquad \beta' = \begin{cases} |\beta| & |\beta| < 45^\circ \\ 90 - |\beta| & |\beta| > 45^\circ \end{cases} \tag{11.2}$$

and d_{cb} is the maximal size of drop diameter above which migration of the drops towards the tube walls due to the buoyant forces takes place (Barnea, 1987):

$$\tilde{d}_{cb} = \frac{d_{cb}}{D} = \frac{3}{8}\frac{\rho_c}{|\Delta\rho|}\frac{f U_c^2}{Dg\cos\beta} = \frac{3}{8} f \frac{\rho_c}{\Delta\rho g} Fr_c; \quad Fr_c = \frac{U_c^2}{Dg\cos\beta} \tag{12}$$

with β denoting the inclination angle to the horizontal (positive for downward inclination). The criterion $\tilde{d}_{max} \leqslant \tilde{d}_{crit}$, with Eqs. (5) and (10), yield a complete transitional criteria to dispersed flows. When the fluids' flow rates are sufficiently high to maintain a turbulence level where $d_{max} < d_{c\sigma}$ and $d_{max} < d_{cb}$, spherical non-deformable drops are formed and the creaming of the dispersed droplets at the upper or lower tube wall is avoided. Thus, the dispersed flow pattern is stable.

Boundary 4 in Fig. 1 corresponds to the results of the H-model when applied with water as the continuous phase, $U_{cs} \equiv U_{ws}$ (oil is dispersed, $U_{ds} \equiv U_{os}$), whereas boundary 5 is obtained when the H-model is applied with oil as the continuous phase $U_{ds} \equiv U_{os}$ (water is dispersed, $U_{cs} \equiv U_{ws}$). It is worth noting that for the critical flow rates along boundary 4, the mixture Reynolds number is already sufficiently high to assure turbulent flow in the water. However, when a viscous oil forms the continuous phase, the locus of the transition to $D_{w/o}$ may be constrained by the minimal flow rates required for transition to turbulent flow in the oil ($Re_c = 2100$ along boundary LT_m). The required turbulent dispersive forces exist only beyond the LT_m boundary, which therefore forms a part of the $D_{w/o}$ transitional boundary.

Inspection of Fig. 1 indicates that when water is considered to form the continuous phase there is a minimal value of the critical water superficial velocity U_{ws}^{o} (U_{ws} for $U_{os} \to 0$) required for establishment of $D_{o/w}$. However, there is a maximal U_{ws}^{*} above which the dispersion stability

criterion implies a stable $D_{o/w}$, irrespective of the oil flow rate. Similarly, when the oil is considered to form the continuous phase, U^{o}_{os} corresponds to the minimal critical oil flow rates for obtaining $D_{w/o}$, whereas U^{*}_{os} corresponds to the maximal oil flow rate below which a flow pattern other than homogeneous $D_{w/o}$ may exist. Thus, for $U_{os} > U^{*}_{os}$ and $U_{ws} > U^{*}_{ws}$, the flow pattern is dispersed flow. In this region, the flow patterns of dispersion of water-in-oil ($D_{w/o}$) and dispersion of oil-in-water ($D_{o/w}$) share a common boundary.

The critical conditions for the establishment of homogeneous dispersion of either oil-in-water (boundary 4) or water-in-oil (boundary 5 and LT_m) are depicted also in Fig. 4, in terms of the critical oil cut as function of the critical mixture velocity (Fig. 4a) or the critical Weber number of the continuous phase, $We_c = \rho_c U_m^2 D/\sigma$ (Fig. 4b). These coordinates are conventionally used in studies of phase inversion phenomena in mixers. In mechanically agitated vessels, the impeller r.p.m, N_I is used for the abscissa and the corresponding dimensionless parameter is $We = \rho_c N_I^2 D_I^3/\sigma$, where D_I is the impeller diameter (U_m is the analogue of $D_I N_I$). In Fig. 4, the two transitional boundaries (curves 4 and 5) that consider the dispersion stability from a dynamical point of view define four zones:

- Zone I—in which the oil cut and the mixture velocity are such that a homogeneous dispersion of the liquids (both $D_{o/w}$ and $D_{w/o}$) is unstable. Other flow patterns must exist.

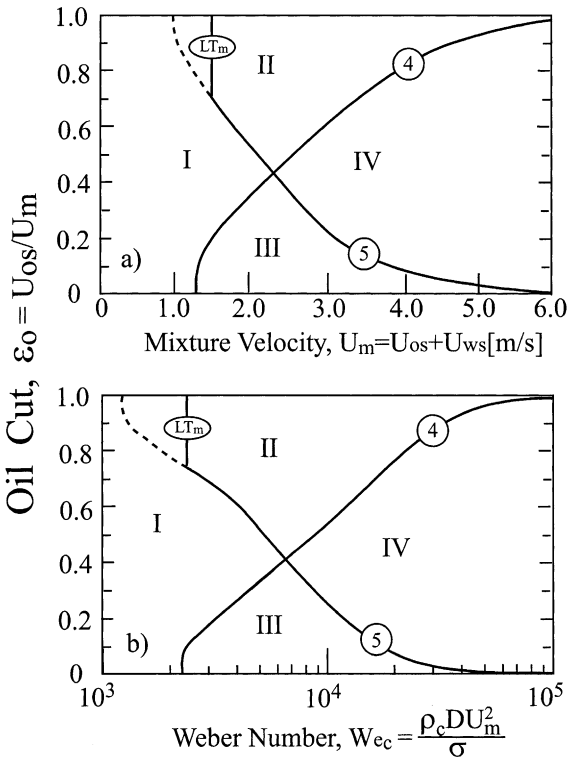

Fig. 4. Fully dispersed flow pattern boundaries: (a) Oil cut vs. mixture velocity; (b) Oil cut vs. Weber number of the continuous phase.

- Zone II—in which the oil cut and the mixture velocity are such that only water can exist as a homogeneously dispersed phase (oil is continuous).
- Zone III—in which the oil cut and the mixture velocity are such that only oil can exist as a homogeneously dispersed phase (water is continuous).
- Zone IV—where either phase can be homogeneously dispersed. Boundaries 4 and 5 provide an upper bound on the width of the ambivalent range.

In Zone IV, the dispersion stability criterion, which is based on dynamical considerations and successfully predicts the transition from dispersed flow to other flow patterns, suggests that both $D_{o/w}$ and $D_{w/o}$ are meta stable. This implies that an additional criterion is required to determine which of the two configurations is the actual pattern expected in the flow system. It is suggested that in this zone, the criterion of the local minimum of the system-free energy can be useful for predicting the conditions under which dynamically stable $D_{o/w}$ will invert into $D_{w/o}$ or vice versa. This inversion will take place in the presence of finite disturbances which are inherent in turbulent flowing systems.

The analysis is performed assuming both the initial dispersion and post-inversion dispersion are homogeneous (with no-slip between the two phases). The drop size and the distance between adjacent drops are considered small compared to the scales used to define the characteristic mixture volume, where local equilibrium is assumed. It is further assumed that compressibility effects are negligible and the temperature is constant, thus, the mixture density (and the system potential energy) is invariant under phase inversion.

3. Phase inversion model

Given a two-fluid (say, oil–water) system and the operational condition, the comparison between the system free energy should refer to two possible configurations of oil dispersed in water ($D_{o/w}$) or water dispersed in oil ($D_{w/o}$). For each of these two configurations, the total free energy consists of the sum of the continuous phase free energy, the dispersed phase free energy and the free energy of the interfaces (formed between the oil and water phases and between the continuous phase and the solid surfaces). Under conditions where the composition of the oil phase and water phase and the system temperature are invariant with phase inversion, the free energy of the oil phase and water phase remain the same. Thus, only the free energies of the interfaces have to be considered.

The surface energy (per unit volume of the mixture) due to the oil–water interface, E_{ow}, is given by:

$$E_{ow} = \varepsilon_d \sigma \frac{\pi \int_0^{d_{max}} d^2 (dN/dd) dd}{\frac{\pi}{6} \int_0^{d_{max}} d^3 (dN/dd) dd} = \frac{6\sigma\varepsilon_d}{d_{32}} \tag{13}$$

where σ is the oil–water surface tension, N is the number of drops with a diameter greater than a specified value d, and d_{32} is the Sauter mean drop diameter.

For oil-in-water dispersion, the total surface energy, Es is thus given by:

$$(Es)_{o/w} = \frac{6\sigma\varepsilon_o}{(d_{32})_{o/w}} + s\sigma_{ws} \tag{14}$$

where $(d_{32})_{o/w}$ is the Sauter mean diameter in $D_{o/w}$, σ_{ws} is the water–solid surface tension coefficient and s is the solid surface area per unit volume. For flow in a smooth pipe, $s = 4/D$. Similarly, for water-in-oil dispersion, the total surface energy is:

$$(Es)_{w/o} = \frac{6\sigma(1-\varepsilon_o)}{(d_{32})_{w/o}} + s\sigma_{os} \tag{15}$$

where $(d_{32})_{w/o}$ is the Sauter mean diameter in $D_{w/o}$, and σ_{os} is the oil–solid surface tension coefficient. Eqs. (14) and (15) assume that the solid surface is completely wetted by the continuous phase.

In view of the physical interpretation and assumptions given above, the flow pattern will be a $D_{o/w}$ under the conditions where such a dispersion is dynamically stable (the criterion $d_{max} < d_{crit}$ is satisfied) and $(Es)_{o/w} < (Es)_{w/o}$. On the other hand, a $D_{w/o}$ will be obtained when such a dispersion is dynamically stable and $(Es)_{w/o} < (Es)_{o/w}$. The phase inversion phenomenon is expected under the critical conditions where both $D_{o/w}$ and $D_{w/o}$ are dynamically stable and the sum of surface energies obtained with either of these two configurations are equal:

$$6\varepsilon_o\left(\frac{\sigma}{d_{32}}\right)_{o/w} + s\sigma_{ws} = 6(1-\varepsilon_o)\left(\frac{\sigma}{d_{32}}\right)_{w/o} + s\sigma_{os} \tag{16}$$

Note that, the difference between the rate of turbulent energy dissipated in the pre- and post-inversion dispersion results in a different characteristic drop size, hence different surface free energy. Using the Young's equation, $\sigma_{os} = \sigma_{ws} + \sigma\cos\theta$, Eq. (16) can be rearranged to yield the critical oil holdup in terms of the liquid–solid surface wettability angle, θ:

$$\varepsilon_o^I = \frac{[\sigma/d_{32}]_{w/o} + \frac{s}{6}\sigma\cos\theta}{[\sigma/d_{32}]_{w/o} + [\sigma/d_{32}]_{o/w}} \tag{17}$$

where $0 \leqslant \theta < 90^\circ$ corresponds to a surface which is preferentially wetted by water (hydrophilic surface), whereas for $90^\circ < \theta \leqslant 180^\circ$ the oil is the wetting fluid (hydrophobic surface).

The Sauter mean drop size can be scaled with reference to the maximal drop size, $d_{32} = d_{max}/k_d$, where k_d is a constant which depends on the fluids system, $k_d \simeq 1.5$–5. It is worth noting that in a recent review by Azzopardi and Hewitt (1997), it has been suggested that the experimental value obtained for k_d may depend on the sample size and for a large number of drops in a sample its value saturates at $k_d \simeq 5$. Using such a scaling, models for d_{max} in $D_{o/w}$ or $D_{w/o}$ can be used in Eq. (17) to evaluate the critical oil holdup at phase inversion. For instance, under conditions where the oil–water surface tension in the pre-inversion and post-inversion dispersions is the same (no surfactants or surface contaminants are involved), $(k_d)_{o/w} \simeq (k_d)_{w/o}$ and solid–liquid wettability effects can be neglected ($\theta = 90^\circ$ or $s \to 0$, as in large diameter pipes, where $d_o, d_w \ll D$), Eq. (17) yields:

$$\frac{\varepsilon_o^I}{1-\varepsilon_o^I} = \frac{d_o}{d_w} \tag{18.1}$$

or

$$\varepsilon_{\mathrm{o}}^{\mathrm{I}} = \frac{d_{\mathrm{o}}/d_{\mathrm{w}}}{1 + d_{\mathrm{o}}/d_{\mathrm{w}}} \tag{18.2}$$

where d_{o} and d_{w} represent the maximal drop size in $D_{\mathrm{o/w}}$ and $D_{\mathrm{w/o}}$ respectively. Thus, if $d_{\mathrm{o}} = d_{\mathrm{w}}$, the critical holdup for phase inversion would be 50%. However, the drop size in both dispersions would be the same only if the physical properties of the two liquids are identical, in particular $\tilde{\rho} = \rho_{\mathrm{o}}/\rho_{\mathrm{w}} = 1$ and $\tilde{\eta} = \eta_{\mathrm{o}}/\eta_{\mathrm{w}} = 1$ (in addition to the above stated assumptions). In order to evaluate $\varepsilon_{\mathrm{o}}^{\mathrm{I}}$ for $\tilde{\rho} \neq 1$ or/and $\tilde{\eta} \neq 1$, models for d_{o} and d_{w} in dense dispersions, as commonly encountered at phase inversion, are required. To that aim, $(d_{\max})_{\epsilon}$ of the H-model (Eq. (7.2)) is employed.

For $D_{\mathrm{o/w}}$, Eq. (7.2) yields:

$$\tilde{d}_{\mathrm{o}} = 7.61\tilde{C}_{\mathrm{H}}\left(\frac{\sigma}{\rho_{\mathrm{w}} D U_{\mathrm{m}}^2}\right)^{0.6}\left(\frac{\rho_{\mathrm{w}} U_{\mathrm{m}} D}{\eta_{\mathrm{w}}}\right)^{0.08}\left(\frac{\rho_{\mathrm{w}}}{\rho_{\mathrm{m}}}\right)^{0.4}\frac{\varepsilon_{\mathrm{o}}^{0.6}}{(1-\varepsilon_{\mathrm{o}})^{0.2}} \tag{19.1}$$

whereas for $D_{\mathrm{w/o}}$ Eq. (7.2) reads:

$$\tilde{d}_{\mathrm{w}} = 7.61\tilde{C}_{\mathrm{H}}\left(\frac{\sigma}{\rho_{\mathrm{o}} D U_{\mathrm{m}}^2}\right)^{0.6}\left(\frac{\rho_{\mathrm{o}} U_{\mathrm{m}} D}{\eta_{\mathrm{o}}}\right)^{0.08}\left(\frac{\rho_{\mathrm{o}}}{\rho_{\mathrm{m}}}\right)^{0.4}\frac{(1-\varepsilon_{\mathrm{o}})^{0.6}}{\varepsilon_{\mathrm{o}}^{0.2}} \tag{19.2}$$

When the ratio of $d_{\mathrm{o}}/d_{\mathrm{w}}$ is of concern, the details of the pipe geometry, the mixture velocity and surface tension (assumed constant) cancel out, whereby:

$$\frac{d_{\mathrm{o}}}{d_{\mathrm{w}}} = \left(\frac{\rho_{\mathrm{o}}}{\rho_{\mathrm{w}}}\right)^{0.12}\left(\frac{\eta_{\mathrm{o}}}{\eta_{\mathrm{w}}}\right)^{0.08}\left(\frac{\varepsilon_{\mathrm{o}}}{1-\varepsilon_{\mathrm{o}}}\right)^{0.8} \tag{20}$$

Combining (20) with (18.1) and (18.2) yields:

$$\frac{\varepsilon_{\mathrm{o}}^{\mathrm{I}}}{1-\varepsilon_{\mathrm{o}}^{\mathrm{I}}} = \tilde{\rho}^{0.6}\tilde{\eta}^{0.4} = \tilde{\rho}\tilde{\nu}^{0.4} \tag{21.1}$$

or

$$\varepsilon_{\mathrm{o}}^{\mathrm{I}} = \frac{\tilde{\rho}\tilde{\nu}^{0.4}}{1 + \tilde{\rho}\tilde{\nu}^{0.4}} \tag{21.2}$$

where $\tilde{\nu}$ is the kinematic viscosity ratio, $\tilde{\nu} = \nu_{\mathrm{o}}/\nu_{\mathrm{w}}$.

4. Model results and discussion

4.1. Comparison with experimental data

Eqs. (20) and (21.2) provide an explanation for the observation made in many experimental studies, that the more viscous phase tends to form the dispersed phase. For a given holdup, and in the case of viscous oil, the characteristic drop size in $D_{\mathrm{o/w}}$ is larger than in the reversed configuration of $D_{\mathrm{w/o}}$. Hence, a larger number of oil drops must be present in order that the surface

energy due to the oil–water interfaces would become the same as that obtained with the water dispersed in the oil. Therefore, with $\tilde{\rho}\tilde{\nu}^{0.4} > 1$, $\varepsilon_o^I > 0.5$, and $\varepsilon_o^I \to 1$ as $\tilde{\rho}\tilde{\nu}^{0.4} \gg 1$. The larger is the oil viscosity, the wider is the range of the oil holdup, $0 \leqslant \varepsilon_o < \varepsilon_o^I$, where a configuration of oil drops dispersed in water is associated with a lower surface energy. In this range of holdups, the flow pattern will be $D_{o/w}$ if the operational conditions are in range where the dynamic stability criterion is satisfied (regions III and IV in Fig. 4). Whereas, $D_{w/o}$ will be obtained in the range of $\varepsilon_o^I \leqslant \varepsilon_o \leqslant 1$, provided such a dispersion is dynamically stable (regions II and IV in Fig. 4). For the oil–water system shown in Fig. 1, Eqs. (21.1) and (21.2), yields $\varepsilon_o^I \simeq 0.78$, which defines the zones of $D_{o/w}$ and $D_{w/o}$ within region IV in Fig. 4 (see also Fig. 7).

For equal density liquids, Eqs. (21.1) and (21.2) is practically the same as Eq. (3) or (4). In Eq. (3) (and in Yeh et al. (1964) model), the power of the viscosity ratio is 0.5. Incidently, the same power (0.5) can be obtained also with the present model: if the friction factor correlation $f = 0.079/Re_c^{0.25}$ is used in Eq. (6.2), the resulting power of Re_c in Eqs. (7.1) and (7.2) is 0.1, and the critical holdup for phase inversion would read:

$$\varepsilon_o^I = \frac{\tilde{\rho}^{0.5}\tilde{\eta}^{0.5}}{1+\tilde{\rho}\tilde{\eta}^{0.5}} = \frac{\tilde{\rho}\tilde{\nu}^{0.5}}{1+\tilde{\rho}\tilde{\nu}^{0.5}} \tag{22}$$

With $\tilde{\rho} = 1$, Eq. (22) is identical to Yeh et al. (1964) model, although its derivation is based on completely different physical picture and arguments. It is further of interest to note, that in order to validate their model, Yeh et al. (1964) did not use a flow system. In their experiments, the liquids dispersions were produced in manually shaken 50 ml flasks. The liquids' density ratio has not been considered as a relevant parameter and was not reported. However, the density of the liquids used in those experiments is available from the International Critical Tables (1928) and the Handbook of Chemistry and Physics (1984). Using Yeh et al. (1964) data and considering the exponents of $\tilde{\rho}$ and $\tilde{\eta}$ in Eq. (22) as parameters linear regression of $\ln[1/\varepsilon_w^I]$ as function of $\ln(\tilde{\eta})$ and $\ln(\tilde{\rho})$ yields the following equation:

$$\varepsilon_o^I = \frac{\tilde{\rho}^{0.37}\tilde{\eta}^{0.3}}{1+\tilde{\rho}^{0.37}\tilde{\eta}^{0.3}} \tag{23}$$

Consulting the 95% confidence intervals on the parameter values indicates that the exponent of the density ratio is not significantly different from zero (0.37 ± 0.86). Ignoring the density ratio in the regression model results in a minor change of the viscosity ratio exponent (0.296 instead of 0.3) with no change of the variance. Indeed, in liquid–liquid systems, where $\tilde{\rho} = O(1)$, the effect of this parameter on the critical holdup may not be very significant (considering the scatter of the data). It is also worth noting that exponent of $\tilde{\rho}$ in Eq. (20) results from the combined effects of three dimensionless groups on the critical drop size (Re_c, We_c and $\tilde{\rho}$ in Eq. (7.2)). Minor changes in the exponents of these dimensionless groups may change the net trend of the dependence of ε_o^I on the density ratio (for instance, if the We_c exponent is 0.5 (instead of 0.6), the effect of $\tilde{\rho}$ in Eq. (22) cancels out). Therefore, the effect of $\tilde{\rho}$ as indicated by the model equations may not be robust. On the other hand, the trend predicted for $\tilde{\eta}$ is robust and reflects the decrease of the drop size with increasing the viscosity of the continuous phase (represented by a positive exponent of Re_c in Eq. (7.2)).

The model developed here implies that a detailed information of the (homogeneous) flow field which produces the dispersions, may not be essential for predicting the critical holdup. For

instance, the intensity of the manual mixing in a flask may not be well controllable. However, as long as the turbulence in the flask is sufficiently intense to provide dynamically stable dispersions, and the container is large enough to diminish solid–liquids wettability effects, the nature of the dispersion (either $D_{o/w}$ or $D_{w/o}$) is determined by the fluids physical properties, whereas the effect of the flow field on the critical holdup practically cancels out.

Fig. 5a shows a comparison of the critical oil holdup predicted via Eq. (21.2), with experimental data of phase inversion in pipe flow reported in the literature (Malinowsky, 1975; Laflin and Oglesby, 1976; Oglesby, 1979; Arirachakaran, 1983; Martinez, 1986). These data were obtained for oil–water flow in pipes of $D = 0.03$ and 0.04 m, $\tilde{\rho} = 0.825$–0.87 and $\tilde{\eta} = 4.9$–1450. The data corresponding to laminar flow in the oil phase is also included in the figure, although the present model considers turbulent flow in the continuous phase for characterizing the drops size. However, since mechanical pre-mixing was used for introducing the viscous oils into the system (Arirachakaran, 1983), the dispersion characteristics were probably determined at the pre-mixing

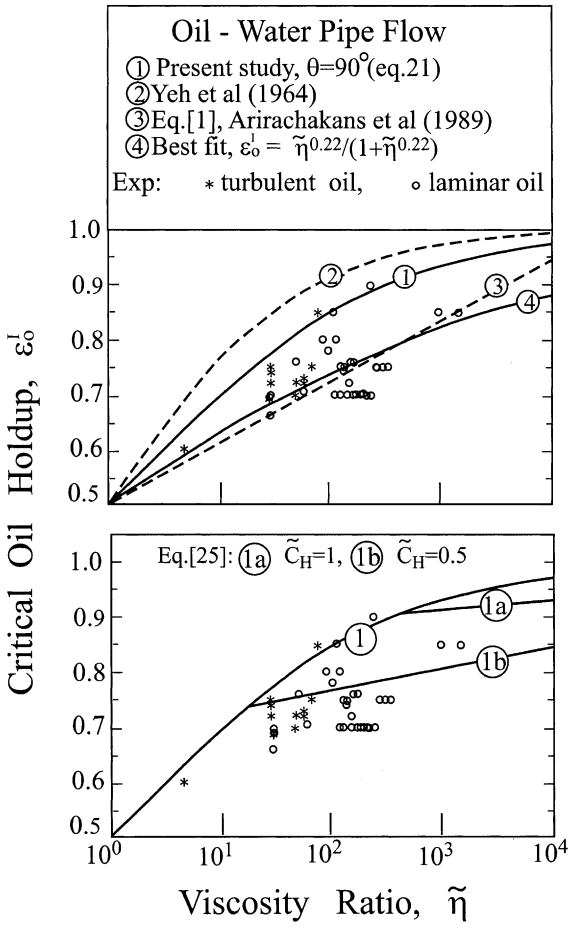

Fig. 5. Comparison of the models predictions with experimental data of the critical oil cut in pipe flow: (a) turbulent and dense $D_{w/o}$, Eq. (21.2), (b) turbulent and dilute $D_{w/o}$, Eq. (25.2).

stage. These data were used by Arirachakaran et al. (1989) to obtain their experimental correlation, Eq. (1) (line 3 in Fig. 5a). A lower variance is however obtained by correlating the data using the form of Eq. (21.2). The best fit (curve 4 in Fig. 5a) indicates an exponent of 0.22 for $\tilde{\eta}$ (when only turbulent oil data is used the exponent is 0.27, the exponent of $\tilde{\rho}$ is again not significantly different from zero). This implies that the form of Eq. (21.2), which is based in mechanistic considerations, is more suitable for correlating experimental data.

4.2. Phase inversion to dilute water-in-oil dispersions

As the viscosity ratio increases, the critical oil holdup increases and reaches high values. Eq. (21.2) predicts that for $\tilde{\eta} \gg 1, \varepsilon_o^I \to 1$. However, for high critical oil holdup, the water-in-oil dispersion is, in fact, dilute. According to the model suggested for evaluating the characteristic drop size, $d_{max} = \max\{(d_{max})_o, (d_{max})_\epsilon\}$. Thus, in dilute $D_{w/o}$, $\tilde{d}_w$ in Eqs. (18.1) and (18.2) (and Eq. (17)) is evaluated based on Eq. (6.1) (instead of Eq. (6.2)). In this case, Eq. (20) should be replaced by:

$$\frac{d_o}{d_w} = 4.0\tilde{C}_H\left(\frac{\rho_o}{\rho_w}\right)^{0.12}\left(\frac{\eta_o}{\eta_w}\right)^{0.08}\left(\frac{\varepsilon_o}{1-\varepsilon_o}\right)^{0.2} \tag{24}$$

Substituting in Eq. (18.1) yields:

$$\frac{\varepsilon_o^I}{(1-\varepsilon_o^I)} = 4\tilde{C}_H\tilde{\rho}^{0.15}\tilde{\eta}^{0.1} \tag{25.1}$$

$$\varepsilon_o^I = \frac{4\tilde{C}_H\tilde{\rho}^{0.15}\tilde{\eta}^{0.1}}{1+4\tilde{C}_H\tilde{\rho}^{0.15}\tilde{\eta}^{0.1}} \tag{25.2}$$

Eq. (25.2), which is the equivalent of Eqs. (21.1) and (21.2) indicates that for for high $\tilde{\eta}$, the critical oil holdup becomes practically independent on the viscosity ratio. It is to be noted that the switch between Eqs. (21.2) and (25.2) depends also on the value of the constant $\tilde{C}_H$. This is demonstrated in Fig. 5b. A value of $\tilde{C}_H \simeq 0.5$ brings the model predictions closer to the cluster of the experimental points in the range high viscosity ratios. The predicted trend is also in accordance with experimental evidences indicating that for highly viscous oils the critical holdup saturates at a value of $\varepsilon_o^I < 1$ ($\varepsilon_o^I \simeq 0.85$, e.g. Brocks and Richmond, 1994). Similar considerations are to be applied when $\tilde{\eta} \ll 1$, where the critical holdup at phase inversion corresponds to dilute $D_{o/w}$. Consequently, the approach of ε_o^I to zero in the limit of $\tilde{\eta} \to 0$, is predicted to be much more moderate than that implied by Eq. (21.2).

Although the experimental data is scattered, the trends shown in Fig. 5 substantiate the applicability of the suggested model for predicting the effect of the oil–water viscosity ratio on the critical holdup. It is also to be noted that the model predictions shown in Fig. 5 correspond to $\theta = 90°$ (or $s \to 0$, negligible liquids/solid-surface wetting effects) and surface tension which is invariant with phase inversion. It will be shown below that when these factors are also considered in the model, the resulting critical holdup for phase inversion is associated with the existence of an ambivalent region, as may be implied by the scattered data in Fig. 5.

For very highly viscous oils, models which are based on turbulent flow with the oil as the continuous phase may be of a limited practical relevance. Therefore, the model given in

Eqs. (21.2) and (25.2) may also be irrelevant for evaluating the drops size of water dispersions in highly viscous oil. Relevant models are those which consider drops deformation and splitting under the action of viscous shear. Such models introduce the capillary number of the continuous phase, $\eta_c U_c/\sigma$ as a dominant parameter instead of the We_c. On the other hand, the Ohnesorge number plays a role in systems of high η_d and/or low surface tension (see Appendix A).

4.3. Ambivalence due to surface rewetting or contaminants

Although the principle of minimization of the system free energy defines a single inversion curve, some ambivalence may still exist around this curve. This ambivalence is herein attributed to processes that follow phase inversion and have a significantly longer time scale (e.g. surface rewetting or diffusion). The resulting ambivalent region is a sub-region of the larger ambivalent zone where both dispersion configurations are meta-stable (zone IV in Fig. 4).

In general, the difference in the wettability of the solid surface by the liquids should be considered in small diameter tubes. Under conditions where the surface energy due to the liquid/solid contact is not negligible, the solution for the critical holdup as obtained by Eq. (17) depends on additional parameters, which include the mixture velocity, the tube diameter, surface tension and liquids/solid wettability angle. The calculation of the critical holdup also requires a value for k_d. The effect of surface wettability is rather small in pipeflow but it is very significant in static mixers (see Section 5).

As indicated by Eq. (17), a hydrophobic surface ($\cos\theta < 0$) affects a reduction of the critical holdup of the organic phase, whereas with hydrophilic surface ($\cos\theta > 0$), the critical holdup of the organic phase increases. The effect of the fluids/solid wetting is more pronounced for larger d/D, thus, in a given system, for lower U_m. This is demonstrated in Fig. 6 using the same oil–water system studied in Figs. 1 and 4. The results in Fig. 6 were obtained for the case in which the liquids surface tension is invariant with phase inversion and $k_d = 2.5$ ($\tilde{C}_H = 1$).

The upper curve in Fig. 6 corresponds to the inversion curve obtained when the tube surface is ideally wetted by water ($\theta = 0$). The lower curve corresponds to the inversion curve for a surface

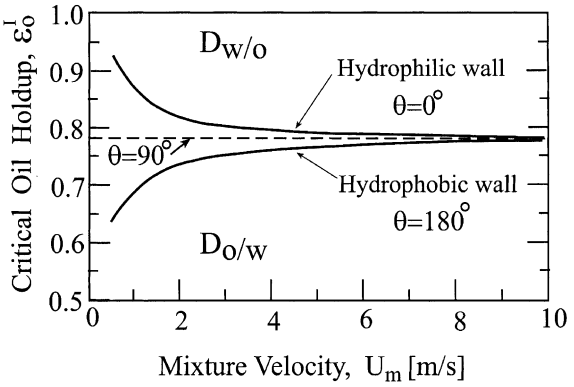

Fig. 6. Region of ambivalence as affected by a change in the liquids/wall wetting-effect of the mixture velocity and contact angle on the critical oil cut for the oil–water system of Fig. 1, ($\tilde{C}_H = 1$, $k_d = 2.5$).

which is ideally wetted by the oil ($\theta = 180°$). As shown, the effect of the wetting characteristics is more significant at lower mixture velocities. For sufficiently high U_m (high We_c), both curves approach the constant critical holdup obtained for $\cos\theta = 0$.

In view of Fig. 6, independently of the surface wetting characteristics, the preferred configuration is water-in-oil dispersion above the upper curve and oil-in-water dispersion below the lower curve. In the region between these two curves, either of the dispersions may exist depending on the liquids wettability. It is to be noted, however, that from the practical point of view, the time scale for complete rewetting of the wall after the inversion (which requires the removal of the old continuous phase film) is much longer than the time scale of the inversion. Consequently, additional meta-stable states (regarding the effective wettability) that are long-lived compared to the time scale of the inversion process are to be considered while applying the principle of the minimization of the system free energy. Start-up procedure and entrance conditions may also affect the effective liquid/surface wettability and thus, the critical conditions for phase inversion. For instance, starting with water as a continuous phase, the wetted tube surface may be considered as practically hydrophilic. In this case, with increasing the oil cut, $D_{o/w}$ is first obtained, which inverts to $D_{w/o}$ along the upper curve. Vice versa, once oil is the continuous phase, in order to invert the $D_{w/o}$ back to $D_{o/w}$, it may be required to reduce the oil cut until the lower inversion curve is reached. Thus, an ambivalent region evolves that is associated with the existence of a hysteresis effect in the phase inversion phenomenon.

Combining Figs. 4 and 6 provides the final definitions of the regions where either $D_{o/w}$ or $D_{w/o}$ are expected (Fig. 7). The wide ambivalent Zone IV in Fig. 4, where both a $D_{o/w}$ and $D_{w/o}$ have been predicted to be stable flow patterns (in view of dynamical considerations) is splitted by the inversion curves into three sub-zones: $D_{o/w}$, $D_{w/o}$ and an narrower ambivalent region. The sub-zone of $D_{o/w}$ merges with Zone III in Fig. 4 to define the operational conditions where the flow pattern is predicted to be $D_{o/w}$, whereas the sub-zone of $D_{w/o}$ merges with Zone II to define the region of $D_{w/o}$. The remaining part of the ambivalent region of Fig. 6 is limited to a narrow range of oil-cut in Fig. 7. In this region, intermittent appearance of the two type of dispersions was observed in the pipe flow (Arirachakaran et al., 1989).

The effect of the liquids viscosity ratio on the ambivalent region due to surface wetting effects is demonstrated in Fig. 8. At a constant U_m, as the viscosity ratio increases, both the minimum oil

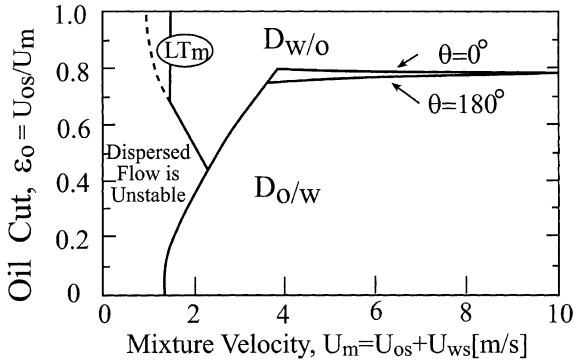

Fig. 7. Regions of $D_{o/w}$ and $D_{w/o}$ as defined by the phase inversion curve for the oil–water system of Fig. 1.

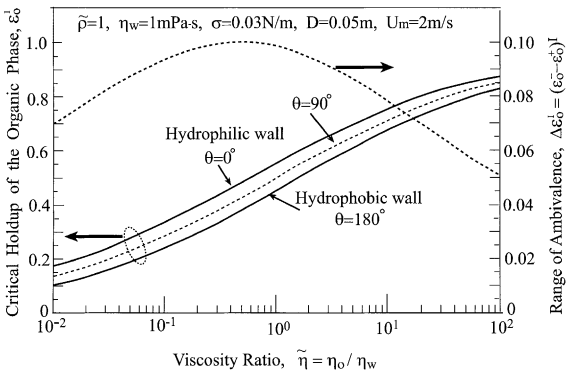

Fig. 8. The effect of the liquids viscosity ratio on the width of the ambivalent region.

volume fraction that can be continuous and its maximum volume fraction that can be dispersed increase. For the constant value of η_w used in Fig. 8, the ambivalent region is the widest for a particular value of the viscosity ratio of about $\tilde{\eta} = 0.5$. A theoretical analysis for the prediction of the value of the viscosity ratio for which the width of the ambivalent region is maximal is given in Appendix B.

The existence of the ambivalent region is not solely attributed to a different free energy of the pipe surface in the initial and post-inversion dispersions. A similar ambivalent region and a hysteresis loop can be expected in any system which is associated with the existence of a free energy term that is independent of the holdup, and exhibit a non-reversible change under phase inversion. The width of such ambivalent region is predicted to increase as that component of the system free energy becomes larger compared to the liquids' interfacial energy. Hence, it widens as the drops become larger (lower liquids viscosities, lower densities, higher surface tension, lower U_m, smaller tube diameter or smaller k_d). The characteristics of such an ambivalent region can be studied by applying a similar analysis to that given in Appendix B.

The discussion so far referred to pure liquid–liquid systems. In pure systems, the liquids' surface tension in the initial dispersion and in the post-inversion dispersion is the same (σ). In such systems, although the inversion phenomenon is attributed to the change in the liquids' interfacial energies, the effect of liquids' surface tension is predicted to be either minor or totally absent (see Eq. (21.2)). It is well known, however, that even the slightest impurities contaminate a two-liquid system. Contaminants, or surfactants accumulate at the liquids' interface and lower the surface tension. However, the diffusion process that eventually leads to recontamination of the 'fresh' drops surface is typically longer than the inversion process (see for example Ullmann et al., 1995). Hence, the surface tension of the contaminated drops in the initial dispersion may be lower than the surface tension of the 'fresh' drops formed at phase inversion. Staring with contaminated oil drops in $D_{o/w}$ with surface tension $\sigma_{o/w} < \sigma$, and following the derivation of Eqs. (17) to (21.1) and (21.2), the equivalent of Eq. (21.2) reads:

$$\frac{\varepsilon_o^I}{1-\varepsilon_o^I} = \tilde{\rho}^{0.6}\tilde{\eta}^{0.4}\tilde{\sigma}^2; \quad \tilde{\sigma} = \frac{\sigma}{\sigma_{o/w}} > 1 \tag{26.1}$$

or

$$\varepsilon_{\mathrm{o}}^{\mathrm{I}} = \frac{\tilde{\rho}\tilde{\nu}^{0.4}\tilde{\sigma}^{2}}{1+\tilde{\rho}\tilde{\nu}^{0.4}\tilde{\sigma}^{2}} \tag{26.2}$$

Thus, a significantly larger oil holdup may be required to invert a contaminated $D_{\mathrm{o/w}}$ into $D_{\mathrm{w/o}}$ compared to the critical oil holdup obtained in a pure system. On the other hand, when contaminated water drops in $D_{\mathrm{w/o}}$ with $\sigma_{\mathrm{w/o}} < \sigma$, invert into $D_{\mathrm{o/w}}$, the equivalent of Eqs. (21.1) and (21.2) reads:

$$\varepsilon_{\mathrm{o}}^{\mathrm{I}} = \frac{\tilde{\rho}\tilde{\nu}^{0.4}\tilde{\sigma}^{-2}}{1+\tilde{\rho}\tilde{\nu}^{0.4}\tilde{\sigma}^{-2}}; \quad \tilde{\sigma} = \frac{\sigma}{\sigma_{\mathrm{w/o}}} > 1 \tag{27}$$

In this case, the oil holdup should be lowered well below the critical holdup corresponding to pure liquids in order to invert the system back to $D_{\mathrm{o/w}}$. Hence, a wide hysteresis gap can be obtained in contaminated oil–water systems, even in large diameter pipes (or large containers), where the surface energy due to liquid/solid contact is negligible. This analysis suggests an explanation to the experimental findings that the presence of contaminates (or surfactants) affects a greater resistance of the system to inversion and considerably increase the limits of ambivalence (e.g. Groeneweg et al., 1998).

Eqs. (26.2) and (27) also demonstrate the fact that when emulsifier is present, it has a controlling effect, which may overshadow the effect of the liquids viscosity ratio and density ratio. It is worth emphasizing, however, that the stabilizing effect of emulsifiers can be much more complex. For instance, effects such as relative partial solubility of the emulsifier in the two phases, its contribution to the formation of an electrical double layer of charge at the interface, and formation of a rigid (or semi-rigid) interfacial film, give rise to additional terms of the free energy that have to be accounted for. In this context, the "surfactant affinity difference", which represents the difference between the chemical potentials of a surfactant in the oil and water phases, can be useful for quantifying the physico-chemical properties of oil/water/surfactant systems and their effect on inversion (Salager et al., 2000). Similarly, the presence of solute, which is not in equilibrium in both phases, may change the free energy of the pre- and post inversion dispersions. Obviously, the inclusion of such additional terms would alter the predicted critical conditions for inversion and the limits of ambivalence.

5. Phase inversion in static mixers

Phase inversion in liquid–liquid systems flowing in a pipe containing an in-line motionless mixer was studied by Tidhar et al. (1986). Mixing elements made of stainless steel and identical elements coated with a film of Teflon were used to study the effect of the liquids/solid surface wetting properties on the critical holdup for inversion. That study indicated a strong influence of the surface material on the phase inversion phenomenon. Indeed, static mixtures are associated with large liquid/surface contact area (large s in Eq. (17)), whereby the liquids/surface wettability is expected to have a significant effect on the critical holdup.

Although, the homogeneous and isotropic turbulence assumptions may not be valid for the flow through static mixers, the Hinze (1955)–Kolmogorov (1949) approach has been found an

appropriate framework for characterizing the experimental data of drop sizes (Middleman, 1974; Tidhar et al., 1986). Following this thrust, the derivation of the model for d_{max} in dilute and dense dispersions formed in a static mixer, follows the same route of that used for obtaining Eqs. (7.1) and (7.2) (see Brauner, 2001). However, the expression introduced for the energy dissipation (per unit volume of the continuous phase), e_c accounts for the higher contact area between the continuous phase and the surface of the mixing elements, whereby:

$$e_c = \frac{\Delta P}{\Delta L}\frac{U_c}{\rho_c(1-\varepsilon_d)} = \frac{1}{2}\frac{\rho_m}{\rho_c(1-\varepsilon_d)}\, s f_c U_c^3 \tag{28.1}$$

or

$$e_c = 2\frac{\rho_m}{\rho_c(1-\varepsilon_d)}\, f_c \frac{U_c^3}{D_h}; \quad D_h = \frac{4}{s} \tag{28.2}$$

where $U_c = 4(Q_d + Q_c)/(\pi D^2 \varepsilon_s)$, and ε_s is the mixing elements' void fraction. Eq. (28.2) introduces the hydraulic diameter, D_h as the characteristic length scale, replacing D in pipe flow. Accordingly, the models for $(d_{max})_o$ and $(d_{max})_\epsilon$ (Eqs. (7.1) and (7.2) are applicable to a static mixer with D_h replacing D everywhere. Hence, the characteristic drop size in $D_{o/w}$, d_o and that in $D_{w/o}$, d_w (needed in Eq. (17)) are given by:

$$\tilde{d}_o = \frac{d_o}{D_h} = 7.61\tilde{C}_H\left(\frac{\sigma}{\rho_w D_h U_m^2}\right)^{0.6}\left(\frac{\rho_w U_m D_h}{\eta_w}\right)^{0.08}\left(\frac{\rho_w}{\rho_m}\right)^{0.4}\frac{\varepsilon_o^{0.6}}{(1-\varepsilon_o)^{0.2}} \tag{29.1}$$

$$\tilde{d}_w = \frac{d_o}{D_h} = 7.61\tilde{C}_H\left(\frac{\sigma}{\rho_o D_h U_m^2}\right)^{0.6}\left(\frac{\rho_o U_m D_h}{\eta_o}\right)^{0.08}\left(\frac{\rho_o}{\rho_m}\right)^{0.4}\frac{(1-\varepsilon_o)^{0.6}}{\varepsilon_o^{0.2}} \tag{29.2}$$

Fig. 9 shows the critical holdup predicted for kerosene–water flow in the static mixer used by Tidhar et al. (1986) in comparison with their data. The upper curve corresponds to the critical kerosene holdup for the case where stainless steel mixing elements are used (for which the reported measured contact angle is 56°). The lower curve corresponds to the critical kerosene holdup for Teflon mixing elements ($\theta = 157°$). The reported values of θ and Eqs. (29.1) and (29.2) were used in Eq. (17) (with $k_d/\tilde{C}_H = 5$). As shown in the figure, the model prediction follow the experimental data points confirming the striking difference between the critical kerosene holdup obtained with the different mixing elements. The region in between the two curves corresponds to $D_{w/o}$ in case Teflon elements are used and to $D_{o/w}$ with stainless steel elements. Consistent with the experimental data, the gap between the two inversion curves becomes wider as U_m decreases. For high U_m, both curves approach asymptotically the critical holdup obtained for $\theta = 90°$ (no solid surface energy), since the surface energy of the mixing elements becomes negligible in comparison to the oil–water interfacial energy associated with the small drops formed at high U_m. The asymptotic value predicted for the kerosene–water system is $\varepsilon_o^I = 0.53$.

It is worth noting that Tidhar et al. (1986) reported on very narrow ambivalent ranges, for each of the two mixers, (indicated by the difference between the open and bold symbols in the figure) that vanish at high velocities. This ambivalence has been characterized by oscillations between oil-continuous and water-continuous configurations which were observed in the flow. The narrow ambivalent range suggests that the rewetting in static mixers is relatively fast.

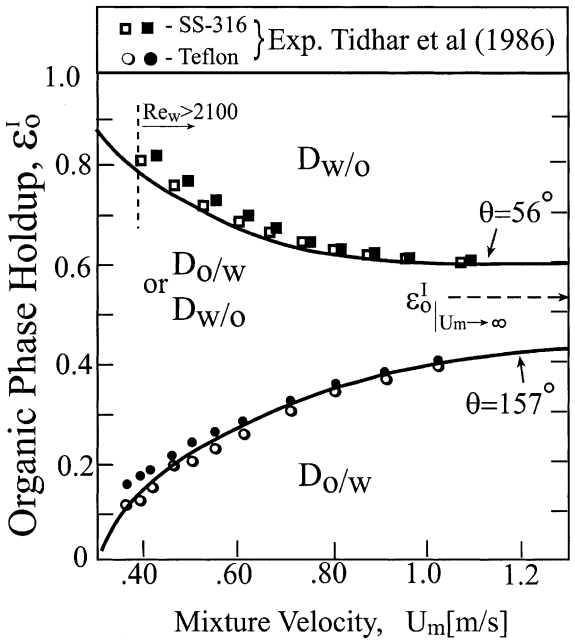

Fig. 9. Effect of liquid/surface wettability on the critical holdup for phase inversion in a static mixer. Comparison of model prediction with experimental data for water–kerosene system (Tidhar et al., 1986).

6. Conclusions

The criterion of the minimum of the system free energy is employed for predicting the conditions under which phase inversion will occur in dispersed two-phase flow systems. The criterion is applied in the range of operational conditions where both the initial dispersion and the post inversion dispersion are judged to be stable in view of a dynamical stability criterion. According to these criteria, when a dispersion structure (say $D_{o/w}$) is associated with higher free energy than that obtained with an alternate structure (say $D_{w/o}$), it will tend to change its structure and eventually reach the one associated with the lowest energy. This hypothesis by itself does not suggest the pertinent dynamical mechanisms by which this transformation occurs. Once such mechanism(s) is identified and modeled, one may be able to follow the dynamics of the transition and in general, one thus has a predictive tool for the phenomenon involved. Such an approach has not been attempted in this study. However, the suggested criteria predict under which conditions phase inversion is expected to occur.

The evaluation of the dispersions free energy requires the availability of models for predicting the characteristic drop size in dense dispersions and its variation with the holdup. This study uses a recent model suggested by Brauner (2001). It is shown that combining this model for drop size in a coalescing, dense dispersion with the criterion of minimum system free energy, yields a model for the critical holdup corresponding to phase inversion, which provides explanations for the experimentally observed features related to phase inversion in pipe flow and in static mixers. These include the effects of the liquids physical properties, liquid/surface wettability (contact angle), the

existence of an ambivalent region and the associated hysteresis loop in pure systems and in contaminated systems. It is shown that when only the liquids' interfacial energy is involved, and the hydrodynamic flow field is similar in the initial and post inversion dispersions, the details of the flow field and the system geometry are not required for predicting the critical holdup at inversion.

Comparisons of the model predictions with experimental data on phase inversion available from the literature show that this model provide a rather simple quantitative tool for evaluating various aspects related to this complicated phenomenon.

Appendix A. Phase inversion in highly viscous oil–water systems

When a highly viscous oil forms the continuous phase, the flow is usually laminar. In laminar pipe flow, the model of Taylor (1964) and Acrivos and Lo (1978) for breakup of long slender droplets in an axisymmetric straining motion can be applied to estimate the characteristic drop size. According to this model for $\eta_d/\eta_c \ll 1$:

$$\frac{d_{max}}{D} = 0.296 \frac{\sigma}{\eta_c \dot{\gamma} D} \left(\frac{\eta_c}{\eta_d}\right)^{1/6} \tag{A.1}$$

where $\dot{\gamma}$ is the strain rate in the continuous phase. In laminar pipe flow, the velocity gradient is a linear function of the radial distance. The average value of $\dot{\gamma}$ is $\dot{\gamma} = 4U_m/D$, whereby Eq. (A.1) yields the following expression for the maximal size of water drops dispersed in a continuous laminar viscous oil flow:

$$\tilde{d}_w = \frac{d_w}{D} = 0.074 \frac{\sigma}{\eta_o U_m} \left(\frac{\eta_o}{\eta_w}\right)^{1/6} \tag{A.2}$$

where $\eta_o U_m/\sigma$ is the capillary number of the oil phase. Eq. (A.2) is applicable in dilute $D_{w/o}$, since the effect of the dispersed phase holdup on the drop size (as accounted in (7.2)) is not included in the model derivation. When Eq. (A.2) is used in Eqs. (18.1) and (18.2) (instead of Eq. (19.2)) the critical oil phase holdup is obtained from the following equation:

$$\frac{\left(\varepsilon_o^I\right)^{0.4}}{\left(1-\varepsilon_o^I\right)^{0.8}} = 105 \tilde{C}_H \frac{(k_d)_{w/o}}{(k_d)_{o/w}} \frac{\eta_w^{0.087}\, \eta_o^{5/6}}{\rho_w^{0.12}\, \rho_m^{0.4}\, \sigma^{0.4}\, D^{0.52}\, U_m^{0.12}} \tag{A.3}$$

In view of Eq. (A.3), due to the different mechanisms of drops breakup in the turbulent flow of $D_{o/w}$, and in laminar flow of $D_{w/o}$, the value of ε_o^I is dependent on the flow field and on all relevant liquids properties. In particular, ε_o^I increases with increasing the oil viscosity (rather than the viscosity ratio) and decreases with increasing the surface tension and the tube diameter. The variation with U_m is rather mild. The critical oil holdup predicted by Eq. (A.3) is demonstrated in Fig. 10) for $U_m = 2$ m/s and $D = 0.04$ m, for which case the continuous oil phase is laminar for $\eta_o > 0.3$ cp ($\tilde{\eta} = 30$). The results were obtained assuming $(k_d)_{o/w} = (k_d)_{w/o}$ (the effect of different values of these parameters and other constant coefficients used in the model are represented by varying the numerical value of the constant, $\tilde{C}_H$). As shown in this figure, this model predicts a steeper increase of the critical oil holdup with increasing the oil viscosity. However, the applicability of the model for $\varepsilon_o^I \ll 1$ is questionable, since for low ε_o^I the water-in-oil dispersion is not

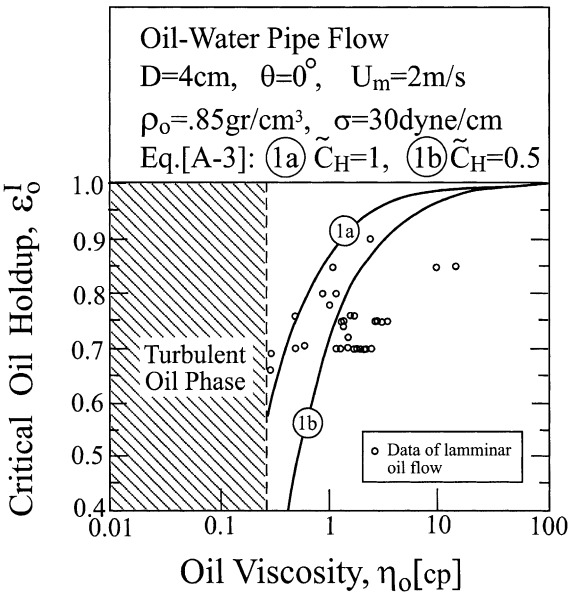

Fig. 10. Comparison of the critical oil cut predicted by the model based on laminar and dilute $D_{w/o}$ (Eq. (A.3)) with experimental data.

dilute. More data of the critical oil holdup at phase inversion in pipe flow of viscous oils (which is not affected by the pre-mixing device) is needed to test these models.

Another modification of the model, which has to be considered in case of a highly viscous oil concerns the effect of the oil viscosity on the drop size in $D_{o/w}$. Eqs. (6.1) and (6.2) (and thus, Eq. (19.1)) has been derived assuming that the main force resisting drop breakage is the surface force due to surface tension and predicts that d_{max} is independent of the dispersed phase viscosity. However, for viscous oils or in systems of low surface tension, additional stabilizing force due to the drop viscosity evolves and results in an increase of d_{max} with increasing η_d. According to Hinze (1955), the viscosity effect is represented by the Ohnesorge number, $On = \eta_d/(\rho_d \sigma d_{max})^{0.5}$. For a non-vanishing On, Eqs. (6.1), (6.2) and (19.1) should be augmented by a term $[1 + f(On)]^{0.6}$, whereby the r.h.s. of Eqs. (20), (24) and (A.3) are also augmented by this term.

Instead, the correction suggested by Davies (1987) can be applied by multiplying these equations by $(1 + K_\eta \eta_d u'_c/\sigma)^{0.6}$, with $K_\eta = O(1)$. The turbulent fluctuation velocity in the continuous phase, u'_c is given by Eq. (4) in Brauner (2001). Note that in the model for $(d_{max})_\epsilon$, this corrrection term evolves when the energy balance used for deriving $(d_{max})_\epsilon$ is modified to account for the additional viscous dissipation rate in the dispersed phase (on top of the rate of surface energy production) required for maintaining the dispersion. Such a modification would affect a steeper increase of the predicted ε^I_o with increasing η_o in systems of $\mu_d u'_c/\sigma > 1$.

The significance of the inclusion of the above correction in the inversion model is tested against the data of Merchuk (2001) for phase inversion in a Water/PEG40000/Phosphate system, obtained in a vortex tube, $D = 1.3$ cm. The surface tension between the two liquid phases in this system is very low, $\sigma < 1$ dyne/cm. The results are summarized in Table 1. It is shown that the critical holdup predicted without the correction due to the dispersed phase viscosity ($K_\eta = 0$, namely Eq. (21.2))

Table 1
Effect of $[1 + k_\eta(\eta_d u'\sigma)]$ correction—comparison with data

ρ (g/cm^3)			η (cp)			σ (Dyne/cm)	Exp. ϵ_2^I	Predicted ϵ_2^I		
ρ_1	ρ_2	ρ_2/ρ_1	η_1	η_2	η_2/η_1			$K_\eta = 0$	$K_\eta = 0.7$	$K_\eta = 1.0$
1.1739	1.0861	0.925	2.095	28.3	13.51	0.62	0.85–0.97	0.73	0.86	0.90
1.1693	1.0790	0.923	2.035	22.3	10.95	0.44	0.86–0.91	0.71	0.84	0.89
1.1410	1.0908	0.956	1.880	21.5	11.44	0.29	0.85–0.92	0.72	0.89	0.95
1.1433	1.0850	0.949	1.930	13.55	7.02	0.15	0.89–0.96	0.68	0.86	0.93

underpredicts the experimental values. The underprediction becomes more pronounced as the surface tension decreases. With the inclusion of the correction term, the predictions are in good agreement with the data. The results for $K_\eta \neq 0$ were obtained with $U_m = 4$ m/s ($Re_2 \approx 2500$). The effect of U_m is however very mild (increasing U_m by a factor of 2 reduces ε_2^I by about 1%).

It is to be noted further that experimental studies in stirred-tank contractors (Wang and Calabrese, 1986) indicate that the effect of viscous resistance of the dispersed phase can be ignored for $Vi = (\eta_d N D_I/\sigma)(\rho_c/\rho_d)^{1/2} \ll We_c^{1/5}$. For a typical oil water-system with $\rho_c \simeq \rho_d$, $\sigma = 30$ dyne/cm and $U_m(\equiv N D_I) = 2$ m/s, this corresponds to $\eta_o \simeq 100$ cp.

Appendix B.

The value of the viscosity ratio for which the width of the ambivalent region ($\varepsilon_o^- - \varepsilon_w^+$) attains a maximum, corresponds to the conditions for which the following Lagrangian is maximal:

$$L = \left(\varepsilon_o^- - \varepsilon_o^+\right) + \lambda_1 F\left(\varepsilon_o^-\right) + \lambda_2 F\left(\varepsilon_o^+\right) \tag{B.1}$$

where ε_o^- and ε_o^+ are the critical oil holdup obtained with hydrophilic surface and hydrophobic surface respectively, and λ_1, λ_2 are the Lagrangian multipliers. The constraints $F(\varepsilon_o^-)$, $F(\varepsilon_o^+)$ results from Eq. (16) when combined with Eqs. (19.1) and (19.2). For hydrophilic wall ($\theta = 0$):

$$F\left(\varepsilon_o^-\right) = -1 + b_1\left(\varepsilon_o^-\right)^{0.4}\left(1 - \varepsilon_o^-\right)^{0.2} - b_2\left(1 - \varepsilon_o^-\right)^{0.4}\left(\varepsilon_o^-\right)^{0.2} \tag{B.2}$$

and for hydrophobic wall ($\theta = 180°$):

$$F\left(\varepsilon_o^+\right) = +1 + b_1\left(\varepsilon_o^+\right)^{0.4}\left(1 - \varepsilon_o^-\right)^{0.2} - b_2\left(1 - \varepsilon_o^+\right)^{0.4}\left(\varepsilon_o^+\right)^{0.2} \tag{B.3}$$

where

$$b_1 = 0.788\tilde{C}_H^{-1} k_d (Ds)^{-1} We_w^{0.6} Re_w^{-0.08}\left(\frac{\rho_m}{\rho_w}\right)^{0.4} \tag{B.4}$$

$$b_2 = 0.788\tilde{C}_H^{-1} k_d (Ds)^{-1} We_o^{0.6} Re_o^{-0.08}\left(\frac{\rho_m}{\rho_o}\right)^{0.4} \tag{B.5}$$

Given the operational conditions and the physical properties of the aqueous phase (b_1 is specified), the extremum of L can be explored by solving the following system of five equations, which represent the conditions for which the Lagrangian defined in Eq. (B.1) is maximal:

$$\frac{\partial L}{\partial \lambda_1} = -1 + b_1\left(\varepsilon_o^-\right)^{0.4}\left(1-\varepsilon_o^-\right)^{0.2} - b_2\left(1-\varepsilon_o^-\right)^{0.4}\left(\varepsilon_o^-\right)^{0.2} = 0 \tag{B.6}$$

$$\frac{\partial L}{\partial \lambda_2} = 1 + b_1\left(\varepsilon_o^+\right)^{0.4}\left(1-\varepsilon_o^+\right)^{0.2} - b_2\left(1-\varepsilon_o^+\right)^{0.4}\left(\varepsilon_o^+\right)^{0.2} = 0 \tag{B.7}$$

$$\frac{\partial L}{\partial \varepsilon_o^-} = 1 + \frac{0.2\lambda_1}{\left[\varepsilon_o^-\left(1-\varepsilon_o^-\right)\right]^{0.6}}\left[b_1\frac{\left(2-3\varepsilon_o^-\right)}{\left(1-\varepsilon_o^-\right)^{0.2}} - b_2\frac{\left(1-3\varepsilon_o^-\right)}{\left(\varepsilon_o^-\right)^{0.2}}\right] = 0 \tag{B.8}$$

$$\frac{\partial L}{\partial \varepsilon_o^+} = -1 + \frac{0.2\lambda_2}{\left[\varepsilon_o^+\left(1-\varepsilon_o^+\right)\right]^{0.6}}\left[b_1\frac{\left(2-3\varepsilon_o^+\right)}{\left(1-\varepsilon_o^+\right)^{0.2}} - b_2\frac{\left(1-3\varepsilon_o^+\right)}{\left(\varepsilon_o^+\right)^{0.2}}\right] = 0 \tag{B.9}$$

$$\frac{\partial L}{\partial b_2} = \lambda_1\left(\varepsilon_o^-\right)^{0.2}\left(1-\varepsilon_o^-\right)^{0.4} + \lambda_2\left(\varepsilon_o^+\right)^{0.2}\left(1-\varepsilon_o^+\right)^{0.4} = 0 \tag{B.10}$$

The five unknowns are: ε_o^-, ε_o^+, λ_1, λ_2 and b_2. The solution indicates that the maximal width of the ambivalent region corresponds to a constant value of the ratio $b_2/b_1 = 0.944 = \tilde{\eta}^{0.08}$ (assuming $\tilde{\rho} \simeq 1$), which yields $\tilde{\eta} = 0.49$ (for $\tilde{\eta} = 1$, $b_2/b_1 = 0.944$ corresponds to $\tilde{\rho} = 0.62$).

It is worth noting, however, that while the maximal width corresponds to a particular b_2/b_1 ratio, its magnitude depends on b_1 (and b_2). The width of the ambivalent region increases as the value of b_1 decreases (almost proportionally to b_1^{-1}). Thus, a wider ambivalent region is obtained for lower liquids viscosities, lower densities, higher surface tension, lower U_m, smaller tube diameter or smaller k_d.

References

Acrivos, A., Lo, T.S., 1978. Deformation and breakup of a single slender drop in an extensional flow. J. Fluid Mech. 86, 641.

Angeli, P., Hewitt, G.F., 1996. Pressure gradient phenomena during horizontal oil–water flow. ASME Proc. OMAE 5, 287–295.

Arashmid, M., Jeffreys, G.V., 1980. Analysis of the phase inversion characteristics of liquid–liquid dispersions. AIChE J. 26, 51–55.

Arirachakaran, S., 1983. An experimental study of two-phase oil–water flow in horizontal pipes, M.S. Thesis, U. of Tulsa, 1983.

Arirachakaran, S., Oglesby, K.D., Malinowsky, M.S., Shoham, O., Brill, J.P., 1989. An analysis of oil/water flow phenomena in horizontal pipes, SPE Paper 18836, SPE Prof. Prod. Operating Symp., Oklahoma.

Azzopardi, B.J., Hewitt, G.F., 1997. Maximum drop sizes in gas-liquid flows. Multiphase Sci. Tech. 9, 109–204.

Barnea, D., 1987. A unified model for predicting flow-pattern transitions for the whole range of pipe inclinations. Int. J. Multiphase Flow 11, 1–12.

Brauner, N., 1998. Liquid–liquid two-phase flows, In: E.V. Schlunder, G.F. Hewitt (Eds.), Section 2.3.5 in HEDH/HEDU Heat Exchanger Design Update.

Brauner, N., 2001. The prediction of dispersed flow boundaries in liquid–liquid and gas–liquid systems. Int. J. Multiphase Flow 27, 885–910.

Brauner, N., 2000. The onset of drops atomization and the prediction of annular flow boundaries in two-phase pipe flow, Internal Report-S101, Faculty of Engineering, Tel–Aviv University, Israel.

Brauner, N., Moalem Moron, D., 1989. Two-phase liquid–liquid stratified flow. Physico-Chem. Hydrodynam. 11, 487–506.

Brauner, N., Moalem Maron, D., 1992. Flow pattern transitions in two-phase liquid–liquid horizontal tubes. Int. J. Multiphase Flow 18, 123–140.

Brauner, N., Moalem Moron, D., Rovinsky, J., 1998. A two-fluid model for stratified flows with curved interfaces. Int. J. Multiphase Flow 24, 975–1004.

Brauner, N., Rovinsky, J., Moalem Maron, D., 1996a. Analytical solution for laminar–laminar two-phase flow in circular conduits. Chem. Eng. Comm. A. Dukler memorial issue., 141–142, 103–143.

Brauner, N., Rovinsky, J., Moalem Maron, D., 1996b. Determination of the interface curvature in stratified two-phase systems by energy considerations. Int. J. Multiphase Flow 22, 1167–1185.

Brocks, B.W., Richmond, H.N., 1994. Phase inversion in non-ionic surfactant-oil–water systems—III. The effect of the oil-phase viscosity on catastrophic inversion and the relationship between the drop sizes present before and after catastrophic inversion. Chem. Eng. Sci. 49, 1843–1853.

Brodkey, R.S., 1969. The phenomena of fluid motions. Addison-Wesley, Reading, MA.

Chesters, A.K., 1991. The modeling of coalescence process in fluid-liquid dispersions: a review of current understanding. Chem. Eng. Res. Des. 69 (A4A), 259–270.

Clarke, S.I., Sawistowski, H., 1978. Phase inversion of stirred liquid/liquid dispersions under mass transfer conditions. Trans. IChemE 56, 50–55.

Das, P.K., Kumar, R., Ramkrishna, D., 1987. Coalescence of drops in stirred dispersion. A white noise model for coalescence. Chem. Eng. Sci. 42, 213–220.

Davies, G.A., 1992. Mixing and coalescence phenomena in liquid–liquid systems. In: Thornton, J.D. (Ed.), Science and Practice of Liquid–Liquid Extraction, vol. 1. Clarendon Press, Oxford, pp. 244–342.

Davies, J.T., 1987. A physical interpretation of drop sizes in homogenizers agitated viscous oils. Chem. Eng. Sci. 42 (7), 1671–1676.

Gilchrist, A., Dyster, K.N., Moore, I.P.T., Nienow, A.W., Carpenter, K.J., 1989. Delayed phase inversion in stirred liquid–liquid dispersions. Chem. Eng. Sci. 44, 2381–2384.

Gorelik, D., Brauner, N., 1999. The interface configuration in two-phase stratified flows. Int. J. Multiphase Flow 25, 977–1007.

Groeneweg, F., Agterof, W.G.M., Jaeger, P., Janssen, J.J.M., Wieringa, J.A., Klahn, J.K., 1998. On the mechanism of the inversion of emulsions. Chem. Eng. Res. Des., Trans. I Chem E (Part A) 76, 55–63.

Guilinger, T.R., Grislingas, A.K., Erga, O., 1988. Phase inversion behavior of water–kerosene dispersions. Ind. Eng. Chem. Res. 27, 878–982.

Handbook of Chemistry and Physics, 1984., 65th ed. Chemical Rubber Publishing Co, CRC Press Inc, Boca Raton, FL.

Hinze, J., 1955. Fundamentals of the hydrodynamic mechanism of splitting in dispersion processes. AIChE J. 1 (3), 289–295.

Hoffer, M.S., Resnick, W., 1979. A study of agitated liquid–liquid dispersions. Part II—Dependence of steady-state dispersion geometry on phase composition and location. Trans. I Chem E 57, 8–14.

International Critical Tables, 1928. 1st ed. vol. 3, McGraw-Hill, New York.

Kato, S., Nakayama, E., Kawasaki, J., 1991. Types of dispersion in agitated liquid–liquid systems. Can. J. Chem. Eng. 69, 222–227.

Kolmogorov, A.N., 1949. On the breaking of drops in turbulent flow. Doklady Akad. Nauk. 66, 825–828.

Kumar, S., 1996. On phase inversion characteristics of stirred dispersions. Chem. Eng. Sci. 51, 831–834.

Kumar, S., Kumar, R., Gandhi, K.S., 1991. Influence of the wetting characteristics of the impeller on phase inversion. Chem. Eng. Sci. 46, 2365–2367.

Laflin, G.C., Oglesby, K.D., 1976. An experimental study on the effects of flow rate, water fraction and gas–liquid ratio on air–oil–water flow in horizontal pipes. M.Sc. Thesis, Université de Tulsa.

Luhning, R.W., Sawistowki, H., 1971. Phase inversion in stirred liquid–liquid systems. Proc. Int. Solvent Extr. Conf. The Hague, Society of Chemical Industry, London, pp. 873–887.

Malinowsky, M.S., 1975. An experimental study of oil–water and air–oil–water flowing mixtures in horizontal pipes. M.Sc. Thesis, Université de Tulsa.

Mao, M., Marsden, S.S., 1977. Stability of concentrated crude oil-in-water emulsions as a function of shear rate, temperature and oil concentration. J. Can. Petrol. 16 (2), 54–59.

Martinez, A.E., 1986. The flow of oil–water mixtures in horizontal pipes. M.Sc. Thesis, Université de Tulsa.

Merchuk, J.C., 2001. Experimental data for phase inversion in Water-PEG4000-Phosphate system. Private communication.

Middleman, S., 1974. Drop size distribution produced by turbulent pipe flow of immiscible fluids through a static mixer. Ind. Eng. Chem. Process Develop. 13, 78–83.

Nädler, M., 1995. The pressure losses in multiphase flow of oil, water and gas in horizontal pipes, Ph.D. Thesis, University of Hanover. Fortschritt-Berichte VDI, Reihe 7: Strömungstechnick No. 296.

Nädler, M., Mewes, D., 1997. Flow induced emulsification in the flow of two immiscible liquids in horizontal pipes. Int. J. Multiphase Flow 23 (1), 55–68.

Norato, M.A., Tsouris, C., Tavlarides, L.L., 1998. Phase inversion studies in liquid–liquid dispersions. Can. J. Chem. Eng. 76, 486–494.

Oglesby, K.D., 1979. An experimental study on the effect of oil viscosity, mixture, velocity and water fraction on horizontal oil–water flow. M.Sc. Thesis, Université de Tulsa.

Pacek, A.W., Moore, I.P.T., Nienow, A.W., Calabrese, R.V., 1994. Video technique for measuring dynamics of liquid–liquid dispersion during phase inversion. AIChE J. 40 (12), 1940–1949.

Pal, R., Bhattacharya, S.N., Rhodes, E., 1986. Flow behaviour of oil-in-water emulsion. Can. J. Chem. Eng. 64, 3–10.

Pan, L., Jayanti, S., Hewitt, G.F., 1995. Flow patterns, phase inversion and pressure gradients in air oil water flow in horizontal pipe. Proc. of the ICMF 95, Kyoto, Japan, paper FT2.

Quinn, J.A., Sigloh, D.B., 1963. Phase inversion in the mixing of immiscible liquid. Can. J. Chem. Eng. 41, 15–18.

Rovinsky, J., Brauner, N., Moalem Maron, D., 1997. Analytical solution for laminar two-phase flow in a fully eccentric core annular configuration. Int. J. Multiphase Flow 23, 523–542.

Salager, J.L., Márquez, L., Peña, A.A., Rondón, M., Silva, F., Tyrode, E., 2000. Current phenomenological know-how and modeling of emulsion inversion. Ind. Eng. Chem. Res. 39, 2665–2676.

Sarkar, S., Phillips, C.R., Mumford, C.J., Jeffreys, G.V., 1980. Mechanisms of phase inversion in rotary agitated columns. Trans. I Chem E 58, 43–50.

Selker, A., Sleicher, Jr., C.A., 1965. Factors affecting which phase will disperse when immiscible liquids are stirred together. Can. J. Chem. Eng. 43 (6), 298–301.

Shinnar, R., 1961. On the behaviour of liquid dispersions in mixing vessels. J. Fluid Mech. 10, 259–275.

Taylor, G.I., 1964. Conical free surfaces and fluid interfaces. Proc. 11th Int. Cong. of Applied Mech., Munich.

Tidhar, M., Merchuk, J.C., Sembira, A.N., Wolf, D., 1986. Characteristics of a motionless mixer for dispersion of immiscible fluids—II. Phase inversion of liquid–liquid systems. Chem. Eng. Sci. 41, 457–462.

Trallero, J.L., 1995. Oil–water flow patterns in horizontal pipes. Ph.D. Thesis, The University of Tulsa, Tulsa.

Ullmann, A., Ludmer, Z., Shinnar, R., 1995. Phase transition extraction process using solvent mixtures with a critical point of miscibility. AIChE J. 41 (3), 488–500.

Vaessen, G.E.J., Visschers, M., Stein, H.N., 1996. Predicting catastrophic inversion on the basis of droplet calescence kinetics. Langmuir 12, 875–882.

Wang, C.Y., Calabrese, R.V., 1986. Drop breakup in turbulent stirred contactors. AIChE J. 32, 667–676.

Yeh, G., Haynie, Jr., F.H., Moses, R.E., 1964. Phase-volume relationship at the point of phase inversion in liquid dispersions. AIChE J. 102, 260–265.

Yeo, L.Y., Matar, O.K., Ortiz, E.S., Hewitt, G.F., 2000. Phase inversion and associated phenomena. Multiphase Sci. Tech. 12, 51–116.